Biochemical and Biophysical Research Communications 436 (2013) 430–435

Contents lists available at SciVerse ScienceDirect

Biochemical and Biophysical Research Communications

journal homepage: www.elsevier.com/locate/ybbrc

Determination of dissociation constant of the NFκB p50/p65 heterodimer using fluorescence cross-correlation spectroscopy in the living cell

Manisha Tiwari, Shintaro Mikuni, Hideki Muto, Masataka Kinjo *

Laboratory of Molecular Cell Dynamics, Faculty of Advanced Life Science, Hokkaido University, Sapporo 001-0021, Japan

ARTICLE INFO

Article history:
Received 21 May 2013
Available online 7 June 2013

Keywords:
NFkB
p50/p65
Dissociation constant
Heterodimer
Fluorescence measurement
FCS/FCCS
Live cell imaging

ABSTRACT

Two-laser-beam fluorescence cross-correlation spectroscopy (FCCS) is promising technique that provides quantitative information about the interactions of biomolecules. The p50/p65 heterodimer is the most abundant and well understood of the NFκB dimers in most cells. However, the quantitative value of affinity, namely the K_d, for the heterodimer in living cells is not known yet. To quantify the heterodimerization of the IPT domain of p50/p65 in the living cell, we used two-laser-beam FCCS. The K_d values of $mCherry_2$- and EGFP-fused p50 and p65 were determined to be 0.46 μM in the cytoplasm and 1.06 μM in the nucleus of the living cell. These results suggest the different binding affinities of the p50/p65 heterodimer in the cytoplasm and nucleus of the living cell and different complex formation in each region.

1. Introduction

The nuclear factor kappa B/Rel family (NFκB/Rel) is a family of inducible transcription factors involved in numerous cellular processes such as immune and inflammatory responses, cell proliferation, apoptosis and development [1–3]. The five members of the mammalian NFκB transcription family are p65 (RelA), RelB, c-Rel, p105/p50 and p100/p52, which associate as homo- and heterodimers [4,5]. The p50/p65 heterodimer is considered the most abundant and best understood complex among the NFκB dimers and plays various roles in gene regulation [3,6]. In unstimulated cells the NFκB p50/p65 heterodimer predominantly exists in the cytoplasm as an inactive complex form with the inhibitor protein IκBα. Upon stimulation, NFκB p50/p65 dissociates from IκBα, translocates to the nucleus and regulates diverse cellular functions [4,7]. A previous report suggested that proteins of this family associate as homo- and heterodimers with different binding affinities for dimerization [8]. The binding affinity of the NFκB p50/p65 heterodimer with DNA has been reported [9,10]. However, the binding affinity of this hetrodimer *in vivo* has not.

To determine the binding affinity of the NFκB p50/p65 heterodimer we calculated the dissociation constants (K_d) of the transiently expressed mCherry tandem dimer ($mCherry_2$) and green fluorescent protein (EGFP) protein fused with IPT (immunoglobulin-like plexin transcription factor) domains of p50 and p65, respectively, in living cells using FCCS. The IPT domain is responsible for dimerization and DNA binding has been reported [8]. Transient transfection is important for expressing the different concentrations of labeled proteins in living U2OS cells. FCCS provides information about the coincidence of two spectrally well-defined fluorescent molecules in a small detection volume with single-molecule sensitivity [11]. The femtoliter confocal volume is well suited to resolve the different measurement positions even in live cells. FCCS has various applications to determine quantitative parameters, including determination of the dissociation constant in the living cell [12–19]. Indeed, single wavelength fluorescence cross-correlation spectroscopy has been employed for determination of dissociation constants [12,13,16]. In this work a two-laser-beam FCSS was used instead of single-beam FCCS because the apparatus is commercially available and it provides more flexible laser power tuning for each fluorescence probe. This gives us adequate fluorescence intensity to reduce pseudo-positive cross-correlation signals that can be caused by the tail of the fluorescence spectrum of EGFP [20]. The technical importance of this work is that flexible laser beam power using two lasers can be applied for any combination of proteins, homo- or heterodimers for analysis of protein dynamics in living cells. Other than FCCS, there

Abbreviations: FCCS, fluorescence cross-correlation spectroscopy; LSM, laser scanning microscopy; EGFP, enhanced green fluorescent protein; $mCherry_2$, mCherry tandem dimer; IPT, immunoglobulin-like plexin transcription factor; NLS, nuclear localization signal; K_d, dissociation constant; NFκB, nuclear factor kappa B.

* Corresponding author. Address: Laboratory of Molecular Cell Dynamics, Faculty of Advanced Life Science, Hokkaido University, N21W11, Kita-ku, Sapporo 001-0021, Japan.

E-mail address: kinjo@sci.hokudai.ac.jp (M. Kinjo).

0006-291X/$ - see front matter © 2013 Elsevier Inc. All rights reserved.
http://dx.doi.org/10.1016/j.bbrc.2013.05.121

are few methods to determine the K_d values of biomolecules in living cells.

In the present study, the dissociation constant of the NFκB p50/p65 heterodimer was determined in the living cell. The results suggest that the NFκB p50/p65 heterodimer has different binding affinities in the cytoplasm and nucleus.

2. Materials and methods

2.1. Plasmid construction

The plasmids encoding p50-mCherry$_2$ and p65-EGFP were constructed by insertion of the encoding sequence of the IPT (immunoglobulin-like plexin transcription factor) domains of p50 and p65 (Fig. S3) into the N-terminal of the tandem mCherry dimer (mCherry$_2$) and EGFP, respectively. For observation of the p50/p65 heterodimer in the nucleus, p50-mCherry$_2$/NLS and p65-EGFP/NLS were constructed. The sequences encoded the SV40 large T antigen nuclear localization signal (Pro-Lys-Lys-Lys-Arg-Lys-Gly) fused with the C-terminal end of mCherry$_2$ or EGFP. Subsequently, the IPT domains of p50 and p65 were inserted into the N-terminals of mCherry$_2$/NLS and EGFP/NLS, respectively. For the cross-correlation positive control experiment, a plasmid encoding the tandem dimer of mCherry and EGFP fusion protein (mCherry$_2$-EGFP) was used. As a negative control, we used plasmids encoding mCherry$_2$ and EGFP simultaneously.

2.2. Cell culture and transient transfection

U2OS cells were grown in a 5% CO_2 humidified atmosphere at 37 °C in McCoy's 5A modified medium supplemented with 10% charcoal-stripped fetal bovine serum, 100 U/mL penicillin G and 100 μg/mL of streptomycin sulfate. For transient transfection, they were placed on Lab-TeK® 8-well chamber cover glass (Nunc™). For FCCS measurement U2OS cells were cotransfected with 200 ng/well p50-mCherry$_2$ or p50-mCherry$_2$/NLS and 100 ng/well p65-EGFP or p65-EGFP/NLS using Optifect™ (Invitrogen). Sixteen hours after transfection, FCCS was performed.

2.3. LSM and FCCS measurement

Confocal LSM imaging and FCCS measurements were carried out with an LSM510-ConfoCor3 (Carl Zeiss) that consisted of a continuous-wave Ar^+ laser and He-Ne laser, a water immersion objective (C-Apochromat, 40 X, 1.2NA; Carl Zeiss) and two channels of avalanche photodiode detectors. This was used for not only FCCS but also LSM imaging. The confocal pinhole diameter was adjusted to 70 μm. EGFP was excited at 488 nm and mCherry at 594 nm. The emission signals were split by a dichroic mirror (600 nm beam splitter) and detected at 505–540 nm for EGFP and at 615–680 nm for mCherry. Measurements in single living cells were performed 10 times for 5 s.

2.4. Data analysis

Data acquired from FCCS were calculated with AIM software (Zeiss, Germany). The fluorescence autocorrelation functions from the green and red channels, $G_G(\tau)$, $G_R(\tau)$, and the fluorescence cross-correlation functions, $G_C(\tau)$, were calculated by

$$G_G(\tau) = 1 + \frac{\langle \delta I_G(t) \cdot \delta I_G(t+\tau) \rangle}{\langle I_G(t) \rangle \cdot \langle I_G(t) \rangle} \tag{1}$$

$$G_R(\tau) = 1 + \frac{\langle \delta I_R(t) \cdot \delta I_R(t+\tau) \rangle}{\langle I_R(t) \rangle \cdot \langle I_R(t) \rangle} \tag{2}$$

$$G_C(\tau) = 1 + \frac{\langle \delta I_G(t) \cdot \delta I_R(t+\tau) \rangle}{\langle I_G(t) \rangle \cdot \langle I_R(t) \rangle} \tag{3}$$

where τ denotes the time delay, I_G is the fluorescence intensity of the green channel, I_R is the fluorescent intensity of the red channel and $G_G(\tau)$, $G_R(\tau)$, and $G_C(\tau)$ denote the autocorrelation functions of green, red and cross, respectively. The acquired auto- and cross-correlations were fitted using a two-component model as follows:

$$G(\tau) = 1 + \frac{1 - F_{\text{triplet}} + F_{\text{triplet}} \exp(-\tau/\tau_{\text{triplet}})}{N(1 - F_{\text{triplet}})} \times \left(\left(\frac{F_{\text{fast}}}{1 + \tau/\tau_{\text{fast}}} \right) \sqrt{\frac{1}{1 + \tau/s^2\tau_{\text{fast}}}} + \left(\frac{F_{\text{slow}}}{1 + \tau/\tau_{\text{slow}}} \right) \sqrt{\frac{1}{1 + \tau/s^2\tau_{\text{slow}}}} \right) \tag{4}$$

where F_{triplet} is the average fraction of triplet state molecules, τ_{triplet} is the triplet relaxation time, F_{fast} and F_{slow} are the fractions of the fast and slow components, respectively, and τ_{fast} and τ_{slow} are the diffusion times of the fast and slow components, respectively. Diffusion constants of the samples were calculated from the ratio of the diffusion constant of Rh6G D_{Rh6G} (414 μm^2/s) [26] and diffusion times τ_{R6G} and τ_{Sample}[27]. In the case of cross-correlation, fitting was performed as $F_{\text{triplet}} = 0$. N is the average number of fluorescent particles in the excitation-detection volume defined by radius (ω_1) and half of the long axis (ω_2) of the confocal volume element, and s is the structural parameter representing the ratio $s = \omega_2/\omega_1$. The values of $\omega_{1,i}$ ($i = G$ or R) are determined from the diffusion coefficients of the rhodamine 6G and Alexa 594 used as standard dyes, respectively.

$$\omega_{1,i} = \sqrt{4D \cdot \tau_{\text{Di}}} \tag{5}$$

The volume elements V are calculated according to

$$V_i = \pi^{3/2} \cdot \omega_{1,i}^2 \cdot \omega_{2,i} \tag{6}$$

$$V_C = \left(\frac{\pi}{2} \right)^{3/2} \left(\omega_{1,G}^2 + \omega_{1,R}^2 \right) \left(\omega_{2,G}^2 + \omega_{2,R}^2 \right)^{1/2} \tag{7}$$

The average numbers of green fluorescent particles (N_G), red fluorescent particles (N_R), and particles that have both green and red fluorescence (N_C) are given by

$$N_G = \frac{1}{G_G(0) - 1} \tag{8}$$

$$N_R = \frac{1}{G_R(0) - 1} \tag{9}$$

$$N_C = \frac{G_C(0) - 1}{(G_R(0) - 1) \cdot (G_G(0) - 1)} \tag{10}$$

when N_G, N_R are constant, $G_C(0)$ is directly proportional to N_C. For quantitative evaluation of cross-correlations among various samples, the relative cross-correlation amplitude (RCA) was calculated as

$$RCA = \frac{G_C(0) - 1}{G_R(0) - 1} \tag{11}$$

To subtract the effect of autofluorescence on N, corrected N ($N_{i,\text{corrected}}$) was calculated by following equation,

$$N_{i,\text{corrected}} = N_{i,\text{measured}} \cdot \left[1 - \frac{I_{i,\text{background}}}{I_{i,\text{measured}}} \right]^2 \tag{12}$$

where $N_{i,\text{measured}}$ is the average number of green or red fluorescent particles obtained from FCCS measurement and fitting analysis ($i = G$ or R). $I_{i,\text{measured}}$ is the average intensity of green or red fluorescence during measurement of FCCS ($i = G$ or R). $I_{i,\text{background}}$ is the

average intensity of green or red fluorescence obtained from FCCS measurement of mock-transfected U2OS cells. Applying the corrected numbers for green and red to Eq. (12), the corrected number of cross correlated particles was calculated as following equation,

$$N_{C,\text{corrected}} = (G_C(0) - 1) \cdot N_{G,\text{corrected}} \cdot N_{R,\text{corrected}} \quad (13)$$

The concentration of each fluorescent protein was calculated with the use of A (Avogadro's number) as given below:

$$[C_{i,\text{corrected}}] = \frac{N_{i,\text{corrected}}}{V_i \cdot A} \quad (14)$$

$$[C_{C,\text{corrected}}] = \frac{N_{C,\text{corrected}}}{V_C \cdot A} \quad (15)$$

Determination of K_d

The dissociation constant K_d was determined using following equations.

$$K_d = \frac{([G_{\text{free}}][R_{\text{free}}])}{[\text{Complex}]} \quad (16)$$

Thus,

$$[G_{\text{free}}] = [C_{G,\text{corrected}}] - [C_{C,\text{corrected}}] \quad (17)$$

$$[R_{\text{free}}] = [C_{R,\text{corrected}}] - [C_{C,\text{corrected}}] \quad (18)$$

$$[\text{Complex}] = [C_{C,\text{corrected}}] \quad (19)$$

The concentrations of the unbound EGFP and mCherry$_2$ fusion proteins [G_{free}] and [R_{free}] were calculated by subtraction of the concentration of the complex [Complex] from the total concentration of the EGFP and mCherry$_2$ fusion protein. For exclusion of the background of cross-correlation, which mainly originated from fluorescent cross talk between two detectors, the data point of less than the average concentration of "Complex" obtained from the negative control were excluded. Then a scatter plot of the products of concentrations of free molecules versus the concentration of the complex was generated with a line of best fit and the dissociation constant (K_d) was calculated from the slope of the regression line [12].

3. Results

3.1. Comparative analysis of cross-correlation of mCherry-EGFP and mCherry$_2$-EGFP in living cell

To examine the cross-correlation of mCherry-EGFP (Fig. 1A) and mCherry$_2$-EGFP (Fig. 1B) fluorescent fusion protein, FCCS was performed in living cells. U2OS cells were transfected with mCherry-EGFP or mCherry$_2$-EGFP fusion proteins. The confocal LSM images of U2OS cells expressing mCherry-EGFP and mCherry$_2$-EGFP fusion proteins showed that both fusion proteins were distributed in the cytoplasm and also in the nucleus (Fig. 2B and D, insets). Typical autocorrelation and cross-correlation curves of FCCS are shown in Fig. 2. As a negative control, U2OS cells were cotransfected independently with mCherry or mCherry$_2$- and EGFP-encoding plasmids. Cross-correlations were not observed (Fig. 2A and C). On the other hand, positive cross-correlation amplitudes were observed in mCherry-EGFP and mCherry$_2$-EGFP (Fig. 2B and D) in FCCS measurement. Furthermore, the amplitude of cross-correlation of mCherry$_2$-EGFP was higher (Fig. 2D) than that of mCherry-EGFP (Fig. 2B). The fluorescent intensity per molecule (count per molecule) of the tandem dimer of mCherry (mCherry$_2$) was also high compared to monomeric mCherry (data not shown). These results indicated that the tandem dimer of mCherry (mCherry$_2$) was advantageous compared to monomeric mCherry in FCCS analysis.

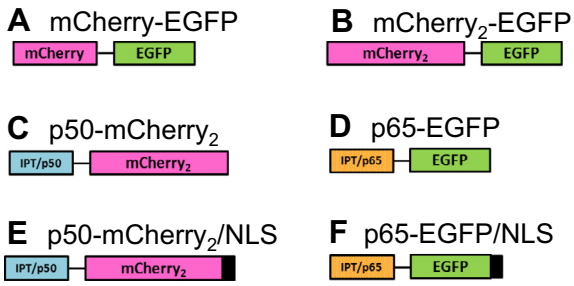

Fig. 1. Schematic diagrams of constructs. (A): mCherry fused with EGFP. (B): Tandem dimer of mCherry fused with EGFP (C): IPT domain of p50 fused with mCherry$_2$. (D): IPT domain of p65 fused with EGFP. (E): IPT domain of p50 fused with mCherry$_2$/NLS. (F): IPT domain of p65 fused with EGFP/NLS. Black region indicates the NLS sequence of SV40.

3.2. FCCS analysis of interaction between p50 and p65 in living cell cytoplasm

To understand the interaction of p50/p65 heterodimers in living cells, U2OS cells were transiently transfected with the IPT domain of p50 fused to mCherry$_2$ (p50-mCherry$_2$) and the IPT domain of p65 fused to EGFP (p65-EGFP) (Fig. 1C and D).

To observe the colocalization of p50-mCherry$_2$ and p65-EGFP in U2OS cells, confocal LSM images were taken. The p50-mCherry$_2$ and p65-EGFP predominantly colocalized in cytoplasm (Fig. 3A, inset). Typical autocorrelation and cross-correlation curves of FCCS measured in the cytoplasm are shown in Fig. 3A. Positive cross-correlation amplitude was observed (Fig. 3A) as in the positive control in FCCS measurement (Fig. 2D). For the semi-quantitative evaluation of cross-correlations the relative cross-amplitude (RCA) was calculated using Eq. (11). Fig. S1A summarizes the RCA in cytoplasm.

For quantitative analysis, the K_d (dissociation constant) of interaction between the p50-mCherry$_2$ and p65-EGFP transiently coexpressing U2OS cells was calculated. The concentrations of fluorescently labeled proteins that both bound [Complex] and free molecules were calculated from the amplitudes of the autocorrelation and the cross-correlation functions in the FCCS analysis using Eqs. (14) and (15). For exclusion of the background of cross-correlation, which mainly originated from fluorescent cross talk between two detectors, some data points of p50/p65 less than the average concentration of "Complex" obtained from the negative control were excluded (Fig. S2). However, no data points were excluded for the p50/p65 heterodimer in this experiment. Then a scatter plot was generated for the product of the concentrations of free molecules [G_{free}][R_{free}] using Eqs. (17) and (18) against the concentration of the bound molecules [Complex] calculated using Eq. (19), and linear regression calculations were used to determine the best fit line through each scatter plot. The K_d was calculated from the slope of the regression line. The K_d of p50-mCherry$_2$ and p65-EGFP was determined to be 0.46 μM in cytoplasm (Fig. 3B). Moreover, the diffusion constant of p65-EGFP was determined from analysis of the fluorescence autocorrelation function fitted with the two-component model. (Fig. 3C) shows a scatter plot of the diffusion constant versus the fraction percentage. As shown in (Fig. 3C), the fraction percentage of the fast component was higher than that of slow component in cytoplasm.

3.3. FCCS analysis of interaction between p50 and p65 in living cell nucleus

Next, we examined the interaction of p50 and p65 in the living cell nucleus. To understand the interaction of p50/p65, U2OS cells were transiently transfected with the IPT domain of p50 fused to

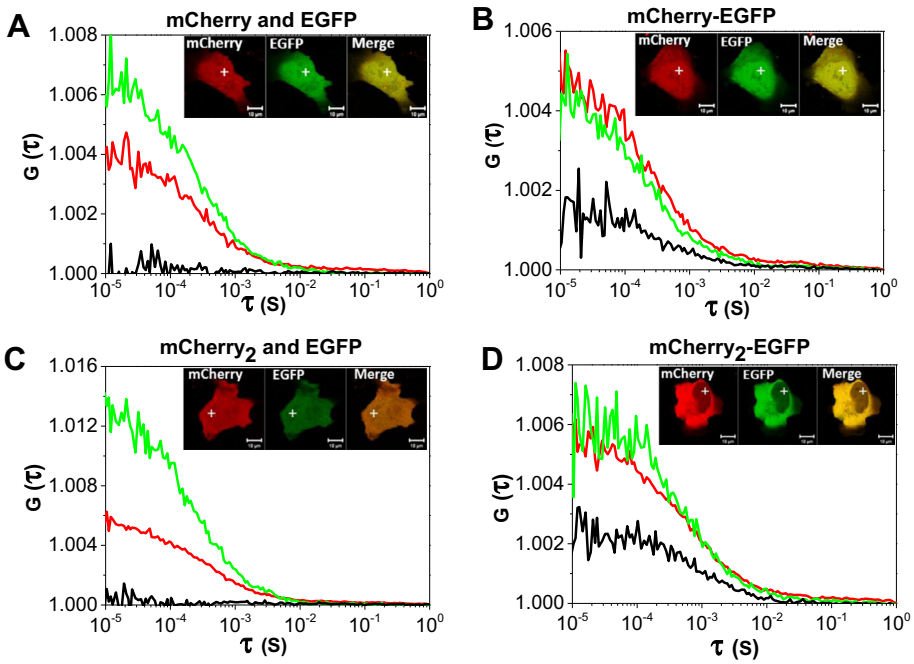

Fig. 2. FCCS measurement of mCherry-EGFP and mCherry$_2$-EGFP Typical auto- and cross-correlation curves were obtained from U2OS cells expressing the pairs of fluorescent fusion proteins. The green, red and black curves denote the autocorrelation of the green channel ($G_G(\tau)$), autocorrelation of the red channel ($G_R(\tau)$),and the cross-correlation curve ($G_C(\tau)$), respectively. The insets show LSM images of U2OS cells expressing the fusion proteins. Measurement positions of FCCS are indicated by the white crosshairs. The scale bar represents 10 μm. FCCS measurement of (A): U2OS cell coexpressing mCherry and EGFP (Negative control) (B): U2OS cell expressing mCherry-EGFP (C): U2OS cell coexpressing mCherry$_2$ and EGFP (Negative control) (D): U2OS cell expressing mCherry$_2$-EGFP.

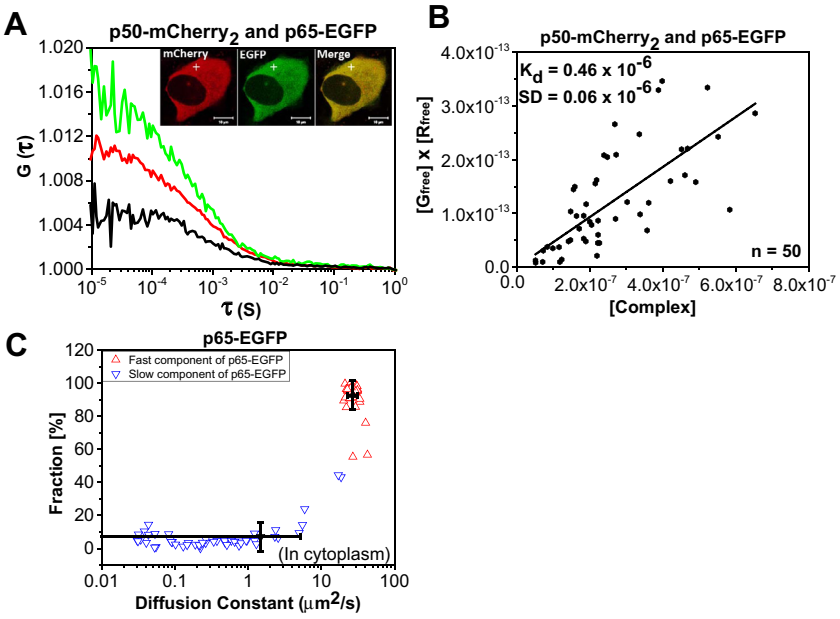

Fig. 3. FCCS measurement and K_d analysis of differently labeled p50 and p65 in cytoplasm of living cells (A): Typical auto and cross-correlation curves were obtained from U2OS cells coexpressing the protein pair of p50-mCherry$_2$ and p65-EGFP in cytoplasm. The green, red and black curves denote the autocorrelation of the green channel ($G_G(\tau)$), autocorrelation of the red channel ($G_R(\tau)$),and the cross-correlation curve ($G_C(\tau)$), respectively. The insets show LSM images of U2OS cells coexpressing the protein pair of p50-mCherry$_2$ and p65-EGFP. Measurement positions of FCCS are indicated by the white crosshairs. The scale bar represents 10 μm. (B): K_d determination results using a scatter plot and linear regression. The plot represents the concentration of the free mCherry$_2$ fusion protein and EGFP fusion protein versus the concentration of the complex of mCherry$_2$ and EGFP fusion proteins. The solid line shows the linear fit. The slope represents the K_d. (C): The scatter plot represents the diffusion constants versus their fractions from FCCS measurement. Black symbols represent the average diffusion constants of the fast and slow components. Error bars represent mean ± SD (n = 50). The open triangles facing up (red) and inverted triangles (blue) represent the fast and slow components, respectively.

mCherry$_2$/NLS (p50-mCherry$_2$/NLS) and the IPT domain of p65 fused to EGFP/NLS (p65-EGFP/NLS) (Fig. 1E and F). As shown in the inset of (Fig. 4B), p50-mCherry$_2$/NLS and p65-EGFP/NLS were localized in the nucleus. As a negative control, FCCS measurement was performed in the nuclei of U2OS cells coexpressing mCherry$_2$/NLS and EGFP/NLS proteins (Fig. 4A inset). Cross-correlation was not observed in FCCS measurement (Fig. 4A), as in Fig. 2C. In contrast, positive cross-correlation amplitude was observed for the p50-mCherry$_2$/NLS and p65-EGFP/NLS protein pair (Fig. 4B). Fig. S1B summarizes the RCA in the nucleus. The K_d

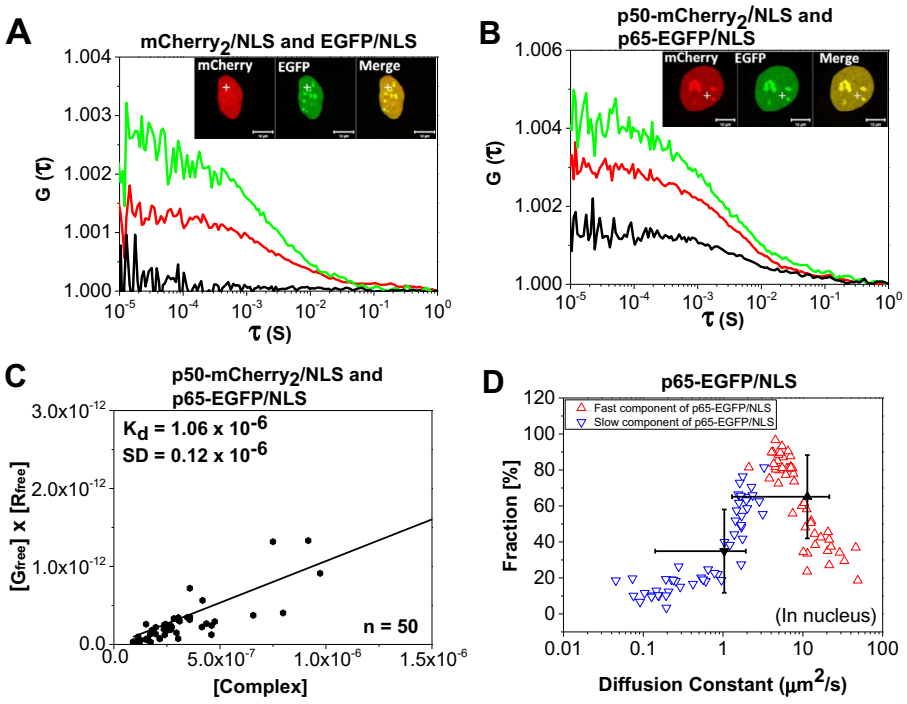

Fig. 4. FCCS measurement and K_d analysis of differently labeled p50 and p65 in living cell nuclei. Typical auto- and cross-correlation curves were obtained from U2OS cells coexpressing the pairs of chimeric fusion proteins. The green, red and black curves denote the autocorrelation of the green channel ($G_G(\tau)$), autocorrelation of the red channel ($G_R(\tau)$), and the cross-correlation curve ($G_C(\tau)$), respectively. The insets show LSM images of the U2OS cells coexpressing the pairs of chimeric fusion proteins. Measurement positions of FCCS are indicated by the white crosshairs. The scale bar represents 10 μm. FCCS measurement of U2OS cells coexpressing, (A): mCherry$_2$/NLS and EGFP/NLS as a negative control (B): p50-mCherry$_2$/NLS and p65-EGFP/NLS. (C): K_d determination results using a scatter plot and linear regression. The plot represents the concentration of the free mCherry$_2$ fusion protein and EGFP fusion protein versus the concentration of the complex of mCherry$_2$ and EGFP fusion proteins. The solid line shows the linear fit. The slope represents the K_d. (D): The scatter plot represents the diffusion constants versus their fractions from FCCS measurement. Black symbols represent the average diffusion constants of the fast and slow components. Error bars represent mean ± SD (n = 50). The open triangles facing up (red) and inverted triangles (blue) represent the fast and slow components, respectively.

of p50-mCherry$_2$/NLS and p65-EGFP/NLS was determined to be 1.06 μM in the nucleus (Fig. 4C), which was higher than that of cytoplasm (Fig. 3B). This result suggested that the binding affinity of the p50/p65 heterodimer in the nucleus was weaker than that in the cytoplasm. The diffusion constant of p65-EGFP was determined from analysis of the fluorescence autocorrelation function fitted with the two-component model. (Fig. 4D) shows a scatter plot of the diffusion constant versus the fraction percentage. As shown in (Fig. 4D), the fraction percentage of the fast component was higher than that of the slow component in the nucleus.

4. Discussion

In this study, we used two-laser-beam fluorescence cross-correlation spectroscopy to estimate the binding affinity of the p50/p65 heterodimer quantitatively in living cells. There are many applications of FCCS to detect bimolecular interactions in solution [21–23]. However, quantitative measurements of interactions are also important in the living cell environment. Quantitative analysis of protein–protein interactions in living cells has been performed by single-wavelength fluorescence cross-correlation spectroscopy [12,13,16], although two-laser-beam FCCS was also used to quantify biological interactions [15,17–19]. In this work, we used two-laser-beam FCCS instead of single-beam FCCS because the two-laser FCCS has more flexible laser power tuning for each fluorescence probe, providing accurate measurement of fluorescence intensity. To our knowledge, there has been no report explaining the binding affinity of the p50/p65 heterodimer in living cells. Here, we determined the dissociation constant of the p50/65 heterodimer in the cytoplasm and nucleus. A fragment of the N-terminal domain of p50 and p65, referred to as the IPT domain, was used in this analysis. It has been reported that this segment is folded into an immunoglobulin-like domain and is responsible for dimerization and DNA binding [8,24]. The high cross-correlation amplitude of p50/p65 interaction in the cytoplasm and nucleus of the living cell was observed (Fig. 3A and Fig. 4B) to have a value similar to that of the positive control (Fig. 2D), suggesting strong interaction of the p50/65 heterodimer. The estimated K_d of this p50/p65 heterodimer was 0.46 μM in cytoplasm (Fig. 3B). On the other hand, the K_d value of the p50/p65 heterodimer was 1.06 μM in the nucleus (Fig. 4C), which was higher than that of cytoplasm, showing the higher binding affinity of the heterodimer in cytoplasm than in the nucleus. This suggested that other molecules might be associated with the p50/p65 heterodimer in cytoplasm to support the complex formation. On the other hand, the complex formation of the heterodimer of p50/p65 *in vitro* is known to be very stable because the crystal structure and refolding of the p50/p65 heterodimer were determined by a dialysis method [6]. The K_d values of the p50/p65 heterodimer and DNA were reported to have high affinity of less than 10 pM [10]. According to these reports, we estimated that the K_d value of p50 and p65 *in vitro* could be less than the pM range because the formation of p50/p65 is stable at concentrations of less than 10 pM. The different values of K_d for p50/p65 formation *in vitro* and *in vivo* might be caused by regulatory or acceleratory molecules for the dissociation. Such lower binding affinity between p50 and p65 heterodimer in the nucleus might suggest more dynamic circumstances of NFκB, which can make a homodimer and/or heterodimer to orchestrate a large number of target genes. Moreover, we found different diffusional properties of the p50/p65 heterodimer in the cytoplasm (Fig. 3C) and nucleus (Fig. 4D). It has been suggested that IκBα binds to the p50/p65 heterodimer with high affinity in cytoplasm [3]. We expected that the

different diffusion properties in cytoplasm would arise due to binding with IκBα and other cytoplasmic proteins.

The diffusion property of p65-EGFP in cytoplasm indicated homogenous distribution of the fast component (Fig. 3C). On the other hand, the variation in the fast component distribution (Fig. 4D) indicated heterogenic interaction in the nucleus. Moreover, compared with the distribution of EGFP/NLS (Fig. S4), the fraction of the slow component of p65-EGFP/NLS was slightly increased. This indicated that the p50/p65 heterodimer interacted with other nucleoplasmic proteins and/or genomic DNA, and that the stability of the heterodimer was weakened by this interaction. However, the detailed mechanisms controlling the stability of p50/p65 in the nucleus were not clarified in this study and need to be further investigated.

Using two-laser-beam fluorescent cross-correlation spectroscopy, we determined the dissociation constant of the p50/p65 heterodimer in living cells. The drawback of two-laser-beam FCCS is the incomplete overlapping of the confocal volume between the green channel and red channel, which leads to reduced cross-correlation [25]. The concentrations of bound molecules [$C_{C,\text{corrected}}$] were obtained using Eq. (19). Eq. (7) is applied for perfect overlap of confocal volume.

In the future, the real overlap value will be determined. However, this will somewhat reduce the value of K_d (unpublished data) though the tendency should be the same. Moreover, we found different binding affinities in the cytoplasm and nucleus of the living cell. Thus, the results presented in this report should be helpful to understand the quantitative interaction of the p50/p65 heterodimer in living cells on the basis of the dissociation constant.

Acknowledgments

This research was partly supported by Grant-in-Aid for Scientific Research (KAKENHI) (S) 21221006 from JSPS, and No. 19058001 in Priority Area "Protein Community" by MEXT.

Appendix A. Supplementary data

Supplementary data associated with this article can be found, in the online version, at http://dx.doi.org/10.1016/j.bbrc.2013.05.121.

References

[1] S. Malek, D.B. Huang, T. Huxford, S. Ghosh, G. Ghosh, X-ray crystal structure of an IB·NF-κB p65 homodimer complex, J. Biol. Chem. 278 (2003) 23094–23100.
[2] B. Berkowitz, D.B. Huang, F.E. Chen-Park, P.B. Sigler, G. Ghosh, The x-ray crystal structure of the NF-κB p50·p65 heterodimer bound to the interferon β-κB site, J. Biol. Chem. 277 (2002) 24694–24700.
[3] C.B. Phelps, L.L. Sengchanthalangsy, T. Huxford, G. Ghosh, Mechanism of IκBα binding to NF-κB dimers, J. Biol. Chem. 275 (2000) 29840–29846.
[4] G. Ghosh, V.Y.F. Wang, D.B. Huang, A. Fusco, NF-κB regulation: lessons from structures, Immunol. Rev. 246 (2012) 36–58.
[5] A. Hoffmann, G. Natoli, G. Ghosh, Transcriptional regulation via the NF-κB signaling module, Oncogene 25 (2006) 6706–6716.
[6] F.E. Chen, S. Kempiak, D.B. Huang, C. Phelps, G. Ghosh, Construction, expression, purification and functional analysis of recombinant NFκB p50/p65 heterodimer, Protein Eng. 12 (1999) 423–428.
[7] R. Fagerlund, L. Kinnunen, M. Kohler, I. Julkunen, K. Melen, NF-κB is transported into the nucleus by importin α3 and importin α4, J. Biol. Chem. 280 (2005) 15942–15951.
[8] D.B. Huang, T. Huxford, Y.Q. Chen, G. Ghosh, The role of DNA in the mechanism of NFκB dimer formation crystal structures of the dimerization domains of the p50 and p65 subunits, Structure (Cambridge, Mass) 5 (1997) 1427–1436.
[9] J.P. Menetski, The structure of the nuclear factor-κB protein-DNA complex varies with DNA-binding site sequence, J. Biol. Chem. 275 (2000) 7619–7625.
[10] T. Fujita, G.P. Nolan, S. Ghosh, D. Baltimore, Independent modes of transcriptional activation by the p50 and p65 subunits of NF-κB, Genes Dev. 6 (1992) 775–787.
[11] F. Sun, S. Mikuni, M. Kinjo, Monitoring the caspase cascade in single apoptotic cells using a three-color fluorescent protein substrate, Biochem. Biophys. Res. Commun. 404 (2011) 706–710.
[12] T. Sudhaharan, P. Liu, Y.H. Foo, W.Y. Bu, K.B. Lim, T. Wohland, S. Ahmed, Determination of *in vivo* dissociation constant, K_D, of Cdc42-effector complexes in live mammalian cells using single wavelength fluorescence cross-correlation spectroscopy, J. Biol. Chem. 284 (2009) 21100.
[13] X.K. Shi, Y.H. Foo, T. Sudhaharan, S.W. Chong, V. Korzh, S. Ahmed, T. Wohland, Determination of dissociation constants in living zebrafish embryos with single wavelength fluorescence cross-correlation spectroscopy, Biophys. J. 97 (2009) 678–686.
[14] P. Liu, T. Sudhaharan, R.M.L. Koh, L.C. Hwang, S. Ahmed, I.N. Maruyama, T. Wohland, Investigation of the dimerization of proteins from the epidermal growth factor receptor family by single wavelength fluorescence cross-correlation spectroscopy, Biophys. J. 93 (2007) 684–698.
[15] J. Savatier, S. Jalaguier, M.L. Ferguson, V. Cavailles, C.A. Royer, Estrogen receptor interactions and dynamics monitored in live cells by fluorescence cross-correlation spectroscopy, Biochemistry 49 (2010) 772–781.
[16] Y.H. Foo, N. Naredi-Rainer, D.C. Lamb, S. Ahmed, T. Wohland, Factors affecting the quantification of biomolecular interactions by fluorescence cross-correlation spectroscopy, Biophys. J. 102 (2012) 1174–1183.
[17] H. Sadamoto, K. Saito, H. Muto, M. Kinjo, E. Ito, Direct observation of dimerization between different CREB1 isoforms in a living cell, PLoS One 6 (2011) e20285.
[18] R. Oyama, H. Takashima, M. Yonezawa, N. Doi, E. Miyamoto-Sato, M. Kinjo, H. Yanagawa, Protein-protein interaction analysis by C-terminally specific fluorescence labeling and fluorescence cross-correlation spectroscopy, Nucleic Acids Res. 34 (2006) e102.
[19] H. Glauner, I.R. Ruttekolk, K. Hansen, B. Steemers, Y.D. Chung, F. Becker, S. Hannus, R. Brock, Simultaneous detection of intracellular target and off-target binding of small molecule cancer drugs at nanomolar concentrations, Br. J. Pharmacol. 160 (2010) 958–970.
[20] H. Sadamoto, H. Muto, Fluorescence cross-correlation spectroscopy (FCCS) to observe dimerization of transcription factors in living cells, Meth. Mol. Biol. 977 (2013) 229–241.
[21] P. Schwille, F.J. Meyer-Almes, R. Rigler, Dual-color fluorescence cross-correlation spectroscopy for multicomponent diffusional analysis in solution, Biophys. J. 72 (1997) 1878–1886.
[22] U. Kettling, A. Koltermann, P. Schwille, M. Eigen, Real-time enzyme kinetics monitored by dual-color fluorescence cross-correlation spectroscopy, Proc. Natl. Acad. Sci. USA 95 (1998) 1416–1420.
[23] F. Fujii, M. Kinjo, Detection of antigen protein by using fluorescence cross-correlation spectroscopy and quantum-dot-labeled antibodies, ChemBioChem 8 (2007) 2199–2203.
[24] C.W. Muller, F.A. Rey, M. Sodeoka, G.L. Verdine, S.C. Harrison, Structure of the NF-κB p50 homodimer bound to DNA, Nature 373 (1995) 311–317.
[25] K. Bacia, P. Schwille, Practical guidelines for dual-color fluorescence cross-correlation spectroscopy, Nat. Protoc. 2 (2007) 2842–2856.
[26] C.B. Muller, A. Loman, V. Pacheco, F. Koberling, D. Willbold, W. Richtering, J. Enderlein, Precise measurement of diffusion by multi-color dual-focus fluorescence correlation spectroscopy, Europhys. Lett. 83 (2008) 46001.
[27] K. Saito, E. Ito, Y. Takakuwa, M. Tamura, M. Kinjo, In situ observation of mobility and anchoring of PKCβI in plasma membrane, FEBS Lett. 541 (2003) 126–131.